Scale selection in columnar joints

Lucas Goehring [*], **L. Mahadevan** [†], **Stephen W. Morris** [* ‡]

[*]Department of Physics, University of Toronto, 60 St. George St., Toronto, Ontario, Canada M5S 1A7, and [†]School of Engineering and Applied Sciences, Harvard University, 29 Oxford Street, Cambridge, MA 02138, USA

Submitted to Proceedings of the National Academy of Sciences of the United States of America

Crack patterns in laboratory experiments on thick samples of drying cornstarch are geometrically similar to columnar joints in cooling lava found at geological sites such as the Giant's Causeway. We present measurements of the crack spacing from both laboratory and geological investigations of columnar jointing, and show how these data can be collapsed onto a single master scaling curve. This is due to the underlying mathematical similarity between theories for the cracking of solids induced by differential drying or by cooling. We use this analogy to give a simple quantitative explanation of how these geometrically similar crack patterns arise from a single dynamical law rooted in the non-equilibrium nature of the phenomena. We also give scaling relations for the characteristic crack spacing in other limits consistent with our experiments and observations, and discuss the implications of our results for the control of crack patterns in thin and thick solid films.

pattern formation | scaling | fracture

Introduction

Drying solids lose moisture from their exposed surfaces and shrink as a consequence. Similarly, cooling solids lose heat from their exposed surfaces and shrink as a consequence. In either case, this differential shrinkage of one part of the solid relative to another leads to stresses that can eventually lead to cracking [1, 2, 3]. While much is known about the nucleation, growth, dynamics and stability of a single crack in an elastic solid, most questions associated with the patterns of multiple cracks due to stresses that arise from non-equilibrium processes such as drying and cooling [4, 5, 6, 7] remain wide open. The resulting polygonal planform patterns can arise in a variety of situations, from the mundane cracks in drying mud, to the deliberately artistic cracks in ceramics and pottery, to the spectacular columnar joint formations of the Giant's Causeway in N. Ireland, Fingal's Cave on Staffa, in Scotland, and the Devil's Postpile in California. The latter formations have fascinated casual observers, artists, and scientists for centuries [8, 9, 10], but no comprehensive physical theory for their form or scale exists. Indeed, it is only in the last decade or so that careful laboratory experiments have started to address the dependence of any of these crack patterns on such quantities as the rate of drying or cooling, the thickness of the layers and their mechanical properties [4, 5, 6, 7, 11, 12, 13]. For example, recent experiments show that crack formation and propagation in drying thin films leads to length scales and patterns that can be strongly time-dependent; cracks in directionally drying films grow diffusively at short times, and can advance intermittently *via* stick-slip like motion over longer times [11, 12]. The patterns formed by these cracks depend in detail on the spatiotemporal dynamics of drying, substrate adhesion and thickness variations [4, 6, 13, 14]. This immediately suggests a non-equilibrium origin to these crack patterns, one that couples the heterogeneous elastic stresses in the cracking solid to the dynamics of drying or cooling, that might be contrasted with the equilibrium crack patterns that are seen and studied in a variety of engineering applications [15].

For columnar joints like those shown in Figure 1, which only occur in relatively thick layers, the similarity between crack patterns induced by drying [16, 17, 18, 19, 20, 21] and cooling [16, 22, 23, 24, 25] can be traced to the fact that the transport of water in a drying slurry and the extraction of heat from a hot solid are mathematically analogous [1, 2, 3]. In a poroelastic medium, fluid flow is coupled to the elastic deformation of a porous solid, while in a thermoelastic medium, heat conduction is coupled to elastic deformation of a conduct-

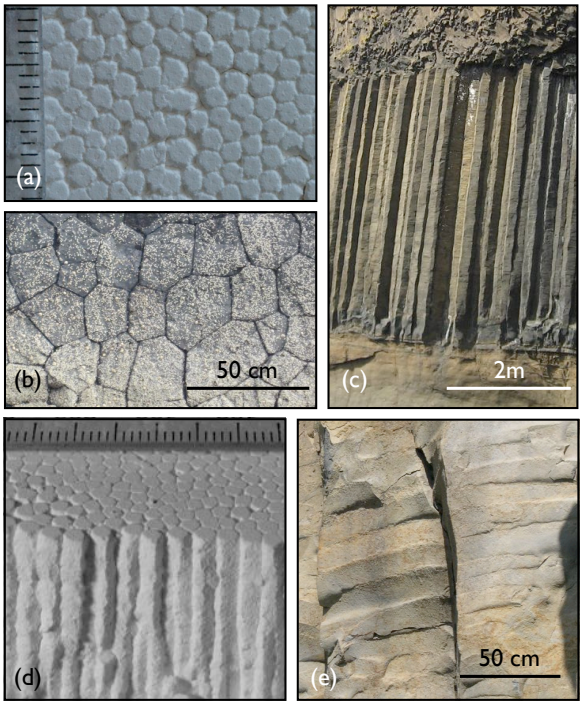

Fig. 1. There is a strong regularity in the pattern of columnar jointing in (a) desiccated corn starch and (b) cooled lava, when observed in cross-section. This roughly hexagonal pattern is caused by a network of shrinkage cracks that organize themselves into an array of almost regular prismatic columns ((c) basalt near Fingals Cave, and (d) corn starch, with a mm scale). (e) the best preserved columnar joints in lava often display striae, chisel-like marks that can be used to infer details of joint formation.

Conflict of interest footnote placeholder

This paper was submitted directly to the PNAS office.

[‡]Email: lg352@cam.ac.uk, lm@seas.harvard.edu, smorris@physics.utoronto.ca

ing solid; pressure in one case is analogous to temperature in the other. In each case, a shrinkage front propagates through the medium leading to the penetration of a crack front that follows slightly behind. Ordering of the crack network at this front carves out the regular columns. In this paper, we shall show how the scale of this shrinkage front sets the average size of the resulting columnar joints. To understand this quantitatively, we present observations on both laboratory and geological columnar joints, and then deduce the appropriate scaling

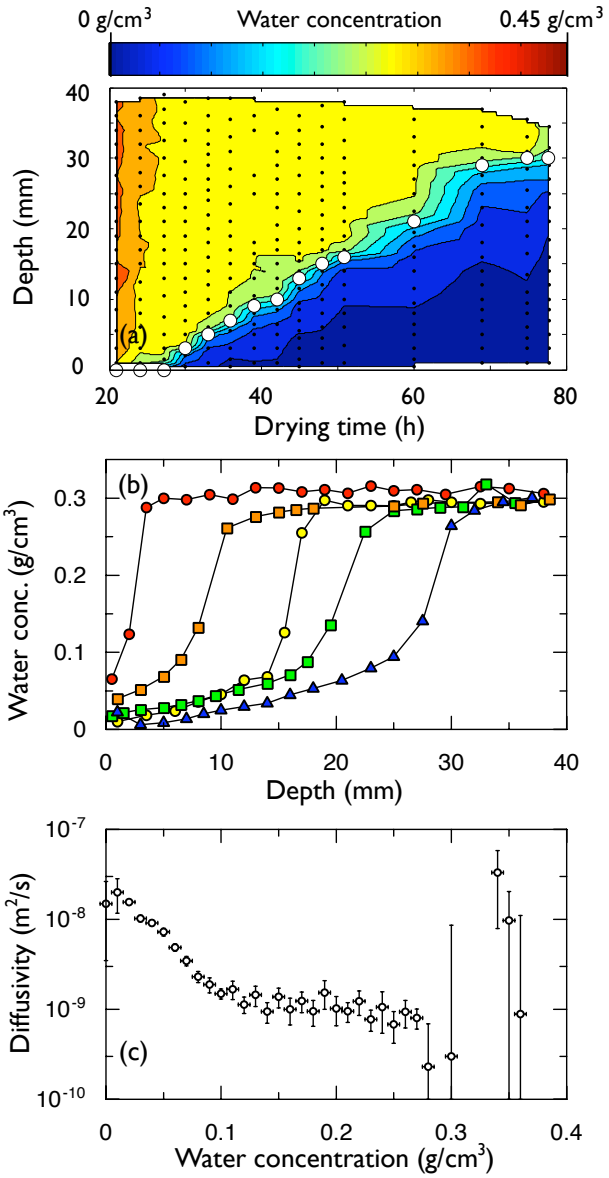

Fig. 2. Drying in starch sets up a travelling desiccation front. (a) Water concentration was measured by weighing small samples taken at various depths from partially dried starch cakes before and after baking the samples dry. In all cases $J_0 = 0.047$ μm/s. Black dots indicate data sampling points and white circles show the position of the fracture front. Background colour shows a linear interpolation of the water concentration field between data. (b) Water concentration distributions 30 h (red), 40 h (orange), 50 h (yellow), 60 h (green), and 70 h (blue) after desiccation is started show that a sharp water concentration front advances through the sample during drying. The drying front is accompanied by a well-defined fracture front propagating at $v = 0.18\mu$m/s. (c) The diffusivity of water in a starch-cake is highly nonlinear. The data show the measured diffusivity, obtained by applying Eqn. 7 to the results shown in (a), averaged over 0.01 g/cm^3 bins, as a function of water concentration.

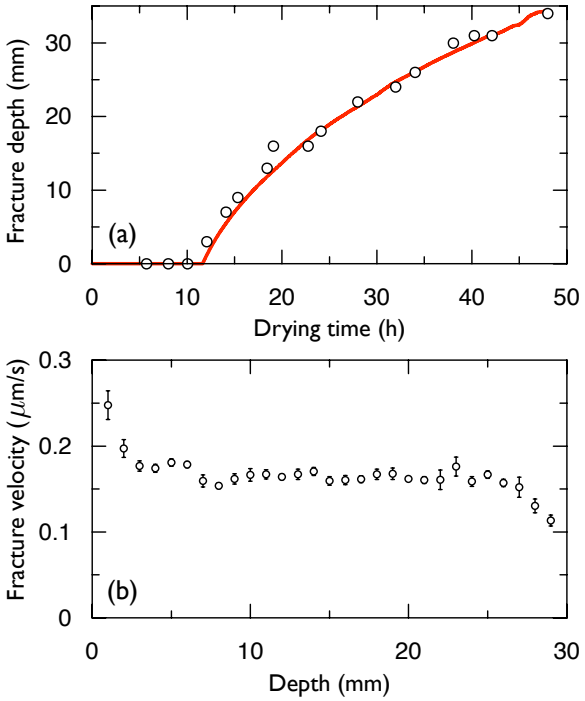

Fig. 3. Inferring fracture position from sample mass measurements in drying starch. (a) Direct measurements (open circles) of the fracture front position, obtained by destructively sampling a series of identical, uncontrolled experiments. These agree very well with the fracture position (red), calculated by inverting records of total sample mass during drying. (b) The derivative of the calculated fracture position can be used to find the average fracture front velocity throughout the starch-cake. In this controlled run, where an evaporation rate of 4.7 μg/cm^{2}s was desired, the average velocity of 0.18 μm/s is nearly constant throughout the sample.

behavior from general theoretical considerations. The resulting scaling law is also applicable to a wide class of fracture problems where the elastic screening length of the crack pattern is smaller than the sample thickness.

Experimental observations on starch

We studied laboratory examples of columnar jointing made by drying slurries of corn starch (see Figure 1(a,d)), that have been known since at least Victorian times [9], although they have only recently been investigated quantitatively [17, 18, 19, 20, 21].

Slurries of corn starch were prepared by mixing equal weights of dry (Canada brand) corn starch and water. Traces of bleach were added to sterilize the experiments, and samples were dried in glass dishes under a pair of 250 W heat lamps. The sample mass was automatically recorded every minute, and this data was used in a feedback loop to control the evaporation rate. If the observed evaporation rate was lower than desired, the duty cycle of the heat lamps was proportionally increased, to deliver more heat to the starch-cake, and *vice versa*. Using these methods, which are described in more detail in Reference [21], we could fix the evaporation rate to within 10% of a desired value throughout the experiment. As discussed below, the evaporation rate controls the rate of fracture advance and the scale of the columns that are formed. In runs with feedback control, the evaporation rate was held constant, and a stable average column size was reached within 1 cm of the drying surface, and maintained

to the base of the starch-cake [21]. In runs without feedback control, the evaporation rate decreases decreased with time, the fracture front slowed and the columns became larger with depth [19, 21, 25]. We measured column scales in both controlled and uncontrolled runs and were thus able to study the column scale over over a wide range of fracture advance rates.

The fracture position as a function of time can be deduced from the sample mass as a function of time using a data inversion technique which integrates the water concentration data, presented in Figure 2(a,b), in order to construct a lookup table for the fracture position as a function of sample mass. Although the exact shape of the water concentration front depends on the evaporation rate (both current and past), these details do not substantially alter the relationship of the total sample mass to fracture position, which reflects the almost step-like jump in water concentration at the drying front, evident in Figure 2(a,b). In order to test this technique, we dried a series of 17 samples under heat lamps, using identical drying conditions for each sample. These were broken open after different drying periods had elapsed, and the fracture position was measured directly in each starch-cake. The sample mass, which had been measured every minute, was then converted into an estimated fracture position using the inversion algorithm. As shown in Figure 3(a), there is excellent agreement between direct observations of the fracture front position, and the position inferred from continuously weighing the starch-cake.

The fracture front velocity v is taken to be the numerical derivative of the fracture position with respect to time. As shown in Figure 3(b), we can use this technique to measure the velocity of the fracture front as it passed through the sample, after drying is complete. Typically, in our controlled experiments, a desired average fracture velocity was well achieved in the middle 60-75% of the sample. The velocity v is simply related to the volumetric flux of evaporated water per unit area J_0 and the sample porosity ϕ by $v = J_0/\phi$. All experiments were consistent with a porosity of $\phi = 26 \pm 1\%$.

Feedback control produced very regular starch joints within a certain narrow size range, using drying fronts that moved through the sample at fixed v. An example is shown in Figure 1(d). To probe a larger range of v, we let thick starch-cakes directionally dry without feedback control, resulting in columns that slowly increase in scale. In both cases, we measured how the fracture spacing, defined as the square root of the average column cross-sectional area, depends on v. Figure 4(a) shows that the fracture spacing is inversely proportional to the instantaneous fracture front velocity v, so that faster drying leads to smaller columns.

Field observations on lava

It is not possible to make direct, dynamical observations on columnar joints as they slowly form in cooling lava flows, although some important insights can be had from borehole temperature measurements that have been made over the decades following the formation of the Kilauea Iki lava lake [26]. It is, however, possible to deduce the cooling rate, fracture advance velocity and column scale from purely geometric characteristics of joints in ancient, exposed flows [25].

We measured columnar joints at field sites across the Columbia Plateau in Washington State, in south-western British Columbia, and on the island of Staffa. The Columbia River Basalt Group covers central Washington state with up to a kilometer of columnar basalt, and extends into Oregon and Idaho [27]. This Miocene flood basalt plateau contains several hundred extensive, chemically homogeneous flows [27, 28]. We used this terrain as a natural laboratory with repeatable lava properties and deposition histories. Nearby, the volcanism of British Columbia allows, in contrast, data to be gathered from highly varied eruption and lava types. Sites in the Garibaldi volcanic belt and the Intermontane belt allowed us to study jointing in this more heterogeneous environment, including the diverse small recent flows of columnar dacite, trachydacite, and alkali basalt in the Vancouver-Whistler corridor [29, 30, 31]. Finally, the lava on the island of Staffa in Scotland is part of the North Atlantic Tertiary Igneous Province, and is compositionally similar to that of the Columbia Plateau, but slightly more basic [32]. We studied the Fingals cave lava unit at several places along the southern coast of Staffa.

At each field site, the average column face width and stria height were measured. Striae are chisel-like marks (see Figure 1(e)), which are left by the individual, sequential fracture advances of a growing crack as it intrudes into the slowly cooling lava [24, 23, 33]. More than a few meters away from any cooling surface, the reflux of water within cracks is the dominant cooling mechanism of lava [26], and establishes a self-sustaining cooling front moving at a constant speed, v.

The temperature gradients near the moving cooling front arise from a competition between the diffusion of heat and the advance of the front at speed v, and it can be shown [25] that they scale inversely with v. The striae leave a permanent record of the temperature field. As each stria forms, the crack tip advances, on average, over a drop in thermal stress given by the tensile strength of the host rock [33, 25]. This implies, in turn, that v and the average stria height are inversely proportional to each other. The coefficient of proportionality linking these terms can be calculated theoretically using the more detailed methods presented in Reference [25]. Here we directly apply this theory, assuming that the physical properties of lavas in all locations were the same as those of the tholeiitic basalts of the Columbia Plateau. Although this is a valid assumption for the Staffa lava, which is compositionally similar to those of the Columbia Plateau, it may contribute to systematic uncertainties in the results from British Columbia.

In general, we found that large columns are due to slower cooling than small columns, consistent with qualitative inferences made previously using crystal texture analysis [22]. Figure 4(b) shows that the fracture spacing of columnar joints in lava is inversely proportional to the speed of the cooling front over a wide range of speeds, and is consistent with the linear relationship between stria height and column face width [25, 34, 23]. We see that the same general relationship between fracture spacing and front speed holds for both cooling lava and drying corn starch slurries. To understand this, we now turn to the mathematical similarity between these physical processes.

Scaling theory

Our dynamic similarity argument rests on the observation that the processes of drying and cooling of a deformable solid are mathematically analogous. In either case, we consider

an elastic solid for which the relative displacement of material is described by a strain tensor $\epsilon = \frac{1}{2}(\nabla u + \nabla u^T)$, where $u(x,t)$ is the displacement vector field. The distribution of internal forces are described by a stress tensor σ, which for a linear elastic solid is simply proportional to the strain, so that $\sigma = \lambda(\nabla \cdot u)I + \mu(\nabla u + \nabla u^T)$, where λ, and μ are the Lamé constants of elasticity. For a conducting solid that is heated or cooled, there is an additional stress and/or strain field due to the changes in temperature. Then the governing equations for thermoelasticity that arise from force balance and conservation of energy lead to

$$\nabla \cdot \sigma = \alpha E \nabla T,$$
$$k\nabla^2 T = \rho C_p \frac{\partial T}{\partial t} + Q\alpha \frac{\partial}{\partial t}(\nabla \cdot u) \qquad [1]$$

where E is the Young's modulus of the solid, α is the coefficient of thermal expansion, k is the thermal conductivity, ρ the density, C_p is the specific heat at constant pressure. The last term characterizes the rate of heat generation due to elastic dilatation and vanishes for thermodynamically reversible deformations, but we leave it here to compare these equations to those for the mechanics of a fluid-infiltrated porous solid where there is an equivalent additional stress due to the movement of liquid within the pores. For a poroelastic solid that has fluid moving relative to the solid through the interstitial pores, the analogous equations are [1, 3, 35]

$$\nabla \cdot \sigma = \beta \nabla p,$$
$$k_h \nabla^2 p = H \frac{\partial p}{\partial t} + \beta K \frac{\partial}{\partial t}(\nabla \cdot u) \qquad [2]$$

where β is a dimensionless elastic constant that relates the local hydraulic pressure to the stress in the porous solid (analogous to the thermal expansion coefficient), k_h is the hydraulic permeability of the porous solid (analogous to the thermal conductivity), H is the effective compliance of the solid which characterizes its softness (and is thus analogous to its "heat capacity"), and K is an appropriately scaled (dimensionless) bulk compressibility of the network [35]. Here the second equation in (2) arises from considerations of Darcy's law for flow through a porous medium, coupled with the equation of mass conservation.

When appropriate boundary conditions are specified for T or p, displacements and/or tractions, the force and energy balance equations completely determine the state of the solid. We see that for a poroelastic solid, pressure is mathematically analogous to temperature, up to factors of the coefficient of thermal expansion and an elastic modulus; indeed the underlying similarity has a thermodynamic origin [1]. Given this, we see that the dynamic similarity of columnar joints in starch and lava arises because the transport of the relevant quantity, water or heat, is essentially diffusive in each case. Indeed, for a linearly elastic isotropic solid the equations (1), yield, in the limit of slow deformations, the uncoupled thermal diffusion equation $\partial T/\partial t = \nabla \cdot (D_T(\nabla T))$, with the thermal diffusivity $D_T = k/\rho C_p$. For poroelasticity, we get an analogous equation of the form $\partial(\nabla \cdot u + \beta p)/\partial t = \nabla \cdot (D_P(\nabla \cdot u + \beta \nabla p))$, with the hydraulic or poroelastic diffusivity $D_P = k_h/H$. We see that the diffusion of heat in thermoelasticity is analogous to the diffusion of water mass content in poroelasticity. To complete the formulation of the problem we need to specify boundary conditions of zero normal traction and a prescribed flux of either heat or moisture on the exposed surface of the half space. Here, we do not solve this problem, but restrict ourselves to a simple testable scaling theory, starting with the case of drying startch, and then transposing our results to the geological problem.

Following an initial transient after a drying/cooling experiment is started, a propagating non-equilibrium steady state of drying/cooling is set up in the solid which leads to the formation of a fracture front that relieves stress in the solid behind it. During the transient drying process near the exposed free surface of a wet, thick starch-cake of large lateral extent, the surface is exposed to low humidity air. After a time t following the beginning of the experiment, a surface layer of thickness L_s shrinks because of the loss of water from it. Shrinkage is easily accommodated in the direction normal to the surface, but leads to an isotropic tensile stress in the plane parallel to it. If the stresses induced by drying are sufficient to exceed some cracking threshold, then cracks will nucleate from the free surface and propagate into the bulk material. Each crack will relieve stress in a region given by the elastic screening or stress relaxation length perpendicular to the crack face, which is proportional to L_s [15]. However, since the drying/cooling field inducing stresses is dynamic, the cracks move from the highly stressed drier surface into the wetter and less stressed bulk, and so slow down and eventually stop. Further drying leads to a repetition of this cycle. Although individual cracks move intermittently via a stick-slip like motion, on average the crack front advances diffusively, following the drying front, albeit slightly behind it [12].

During the initial phase of drying near the surface of a very thick sample, approximated as a half-space, the only dynamical length scale that arises naturally is given by

$$L_s \sim (D_P t)^{1/2} \qquad [3]$$

where D_P is the poroelastic diffusivity characterizing the equilibration of fluid mass content. If the evaporative flux J_0 decreases with time, as in the case when the external humidity is kept constant, the crack front slows as the transport of water is limited by diffusion out the sample. As time progresses, L_s increases and the crack pattern should coarsen, *i.e.* the crack spacing should increase with increasing distance from the exposed surface. This coarsening has been previously noticed in starch experiments [17, 19, 20]. Our explanation for the coarsening follows from the non-equilibrium nature of drying/cooling as outlined above, in sharp contrast with equilibrium theories given hitherto for these crack patterns which are based on free energy minimization [36]. When the evaporation rate is kept constant, so that the volumetric flux J_0, is invariant in time, we find ourselves in a non-equilibrium steady state. This is achieved in the flux-controlled starch experiments presented earlier, where after a transient near the surface, the crack spacing does not coarsen further. Achieving this steady state requires that the drying power increase with time. In this case, the drying front progresses into the sample at a constant speed v. Under these conditions, the elastic stress screening length is also invariant, and scales as

$$L_s \sim D_P/J_0 \qquad [4]$$

This allows us to define a dimensionless Péclet number for a crack spacing L_c,

$$\mathrm{Pe} = vL_c/D_P \qquad [5]$$

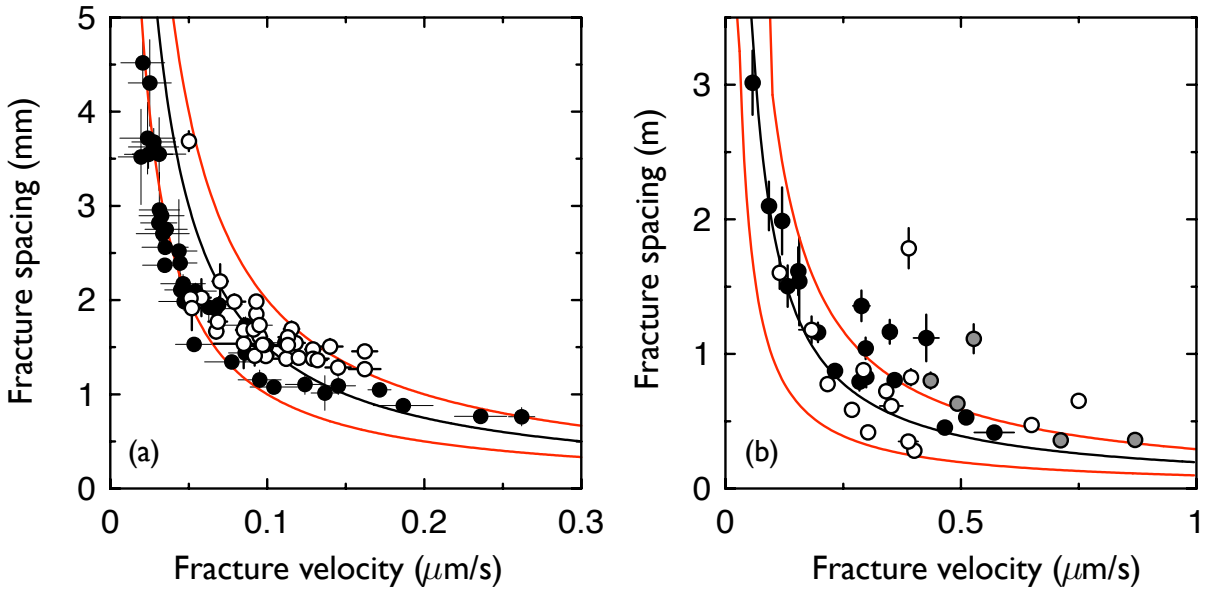

Fig. 4. The average fracture advance speed, v, and the fracture spacing of columnar joints, L_c, are inversely related. This relationship is described by a Péclet number, Pe, the product of v and L_c, normalized by the diffusivity of moisture or temperature in the system. (a) shows fracture spacing from desiccated starch experiments. Closed circles show the fracture spacing in two deep samples as it coarsens in response to a gradually slowing drying front. Open circles show the final fracture spacing that was selected in individual experiments in which the evaporation rate was kept constant throughout drying. Solid lines indicate curves of constant Pe = 0.1, 0.15, and 0.2. (b) shows fracture spacing from field observations in the tholeiitic basalt of the Columbia River Basalt Group (black circles), and the Island of Staffa (grey circles), and from a range of columnar lavas types found in South-Western British Columbia (open circles). Solid lines indicate an inverse dependence of fracture spacing on fracture velocity, showing the curves Pe = 0.15, 0.3, and 0.5.

where the drying front velocity v is related to the moisture flux J_0 and the porosity ϕ by $v = J_0/\phi$. Since $\mathrm{Pe} \sim L_c/L_s$, the observed inverse scaling of fracture spacing to fracture advance rate follows if jointing proceeds at a constant $\mathrm{Pe} \sim O(1)$.

Similar considerations apply to the lava cooling case, with the poroelastic diffusivity D_P replaced by the thermal diffusivity $D_T = k/\rho C_p$. In the case of cooling lava, coarsening has been observed near the flow margin [23], while the non-equilibrium steady state is maintained far away from the flow margin by the heat transport due to the reflux of water in the cracks [24, 25, 26]. In this regime, a very regular column scale is observed as in Figure 1(c,d).

The dynamic similarity of starch and lava columns

Our scaling theory simplifies somewhat the drying process in the starch experiment; the relationship between the local water concentration C and the pressure p is somewhat complicated by the fact the pores are not fully saturated with water, but instead consist of water bridges, air and water vapor. During the drying process, water is transported under the pressure gradient predominantly as liquid at the wet end of the sample, and predominantly as vapor near the dry end [37, 20]. Since linear poroelasticity theory shows that the water mass content satisfies a linear diffusion equation, we expect that the moisture concentration C, which we measured directly in the experiments, also obeys a diffusion equation. However, given the large variations in water content that lead to fundamentally different mechanisms for moisture transport at early and late times [37], the diffusivity is a function of the moisture content in the solid so that C now satisfies a nonlinear diffusion equation of the form

$$\nabla \cdot [D(C)\nabla C] = \frac{\partial C}{\partial t}, \qquad [6]$$

where $D(C)$ is a concentration-dependent effective diffusivity (related to the poroelastic diffusivity $D_P \sim k_h/H$) which can be deduced from the experimental data.

In our starch experiments, we controlled the volumetric flux of water J_0 at the surface, rather than the vapor pressure p. We sampled the moisture concentration $C(z,t)$ in the vertical direction z in many identical starch-cakes dried for different times t, by sectioning the cakes into 1-2 mm thick layers, and weighing, drying, and reweighing the sections. As shown in Figure 2(a), the cakes dried uniformly to a critical moisture concentration of 0.30 g/cm^3, after which time a sharp drying front was initiated at the upper drying surface. Below this front, C remained constant. As the drying front steadily advanced, it maintained a concave, self-similar shape, as shown in Figure 2(b). To understand this, we consider Eqn. 6 which can be integrated to give the concentration-dependent diffusivity [37],

$$D(C(z,t)) = \left(\int_h^z \frac{\partial C}{\partial t} dz'\right) \Big/ \left(\frac{\partial C}{\partial z}\right). \qquad [7]$$

Here we have assumed one dimensional transport, and that the sample lies in $0 \le z \le h$. We have imposed a no-flux boundary condition on the lower boundary $z = h$, which is in contact with the base of the container. Figure 2(c) shows the effective diffusivity $D(C)$ as calculated from Eqn. 7 and the water concentration data presented in Figure 2(a). There is a broad minimum in $D(C)$, reaching $D_0 = 1.1 \times 10^{-9}$ m^2/s over approximately $C = 0.1 - 0.3$ g/cm^3. Above a concentration of 0.3 g/cm^3 the diffusivity must continue to increase with C, as the starch-cake dries almost uniformly from saturation down to this concentration. However, under these wet conditions, $\partial C/\partial x$ is very small and these data cannot be reliably used to find $D(C)$. The minimum in $D(C)$, which

we call D_0, is due to the crossover between liquid and vapor transport [37] which occurs at the sharp drop-off in water concentration which forms the drying front. It is therefore this minimum D_0 which is relevant to the scaling of the columns. Using Eqn. 5 with $D_P = D_0$, the measured starch fracture spacing shown in Figure 4(a) is thus found to correspond to a range of Péclet numbers $\mathrm{Pe} = 0.15 \pm 0.05$.

In the case of lava, the energy balance Eqn. 1, reduces to a linear diffusion equation with a diffusivity $D_T = k/\rho C_p$. Then, we transpose the result for drying starch to the case of cooling lava by reinterpreting D as the thermal diffusivity D_T and J_0 as the heat flux which is strongly influenced by the continuous reflux of water in the cracks [24, 25], although this effect does not significantly influence the water transport in the case of drying starch [21]. Since the thermal diffusivity of basalt [25] is approximately $D_T = 6.5 \times 10^{-7}$ m^2/s, and the fracture front velocities are comparable to those in the starch experiments, columnar jointing in lava should be 10-100 times larger than in starch. We see that this is indeed the case, as shown in Figure 4(b); jointing in lava is well described by $\mathrm{Pe} = 0.3 \pm 0.2$, very similar to that found in the starch experiments.

Discussion

Our simple scaling theory embodied in Eqns. 3-5 provides a unified way of understanding the basic observations of columnar jointing induced by the non-equilibrium and inhomogeneous cooling in a geological context, and *via* a mathematical analogy, the columnar jointing in laboratory experiments of the drying of a fluid infiltrated porous solid such as starch. In particular, we are able to derive a simple scaling law for the crack spacing consistent with both previous and current experimental observations.

In addition to explaining an old geological mystery, and connecting it to a number of everyday observations of cracking, our work paves the way for the engineered cracking of solids to obtain patterns at will. To take one example, in the production of fine coke from crushed coal, it is the cooling-induced shrinkage cracks that control the size, and hence quality, of the product [38]. Other applications range from the industrial drying of paint, concrete, and photographic paper, to mud-cracks and the desiccation of soils, the thermal fracture of permafrost [39], and the jointing of metamorphic rocks [40]. In all of these examples, the crack patterns are controlled by the competition between non-equilibrium processes such as the relatively slow drying and cooling, by which stresses develop, and rapid cracking which causes these stresses to be relieved. Thus although elastic deformation is important, the dynamics of crack propagation are much faster than the much slower process of stress generation which ultimately determines the rate of cracking and thence the scale of jointing.

We conclude with a brief discussion of the drying or cooling of a solid of finite thickness h. For very thin or very slowly cooling (or drying) solids, the crack spacing will be $\sim O(h)$, if cracks form at all [4, 5, 13]. However, if the characteristic scale given by Eqn. 3 is smaller than h, the fracture spacing $\sim L_s$, no longer depends on h, but is instead a function of the cooling (or drying) rate. More generally, if the characteristic elastic stress screening length is smaller than the thickness of the drying solid, then the crack spacing is just the stress relaxation length, so that the crack spacing should be proportional to $min(h, L_s)$.

The authors thank Catherine Duquette, Robert Mehew, and Brian Goehring for their assistance in the field, National Trust for Scotland for allowing extended access to Staffa, and to Pierre-Yves Robin, Mark Jellinek, and Kelly Russell for their advice on geology.

1. Biot M A (1941) General theory of three-dimensional consolidation. *J App Phys* 12:155–164.
2. Norris A (1992) On the correspondence between poroelasticity and thermoelasticity. *J Appl Phys* 71:1138–41.
3. Boley B A, Weiner J H (1960) *Theory of thermal stresses.* (Wiley, New York), p. 586.
4. Groisman A, Kaplan E (1994) An experimental study of cracking induced by desiccation. *Europhys Lett* 25:415–20.
5. Allain C, Limat L (1995) Regular patterns of cracks formed by directional drying of a colloidal suspension. *Phys Rev Lett* 74:2981–2984.
6. Shorlin K A, de Bruyn J R, Graham M, Morris S W (2000) Development and geometry of isotropic and directional shrinkage crack patterns. *Phys Rev E* 61:6950–6957.
7. Yuse A, Sano M (1993) Transition between crack patterns in quenched glass plates. *Nature* 362:329–331.
8. Bulkeley R (1693) Part of a letter from Sir R.B.S.R.S. to Dr. Lister, concerning the Giants Causway in the County of Atrim in Ireland. *Phil Trans R Soc Lond* 17:708–710.
9. Huxley T H (1881) *Physiography: An Introduction to the Study of Nature.* (MacMillan and Co., London), p. 204.
10. Kennedy A (2007) In search of the 'true prospect': making and knowing the Giant's Causeway as a field site in the seventeenth century. *Brit J Hist Sci* pp. 1–24, in press.
11. Dufresne E R, Corwin E I, Greenblatt N A, Ashmore J, Wang D Y, Dinsmore A D, Cheng J X, Xie X S, Hutchinson J W, Weitz, D A (2003) Flow and fracture in drying nanoparticle suspensions. *Phys Rev Lett* 91:224501.
12. Dufresne E R, Stark D J, Greenblatt N A, Cheng J X, Hutchinson J W, Mahadevan L, Weitz D A (2006) Dynamics of fracture in drying suspensions. *Langmuir* 22:7144–7147.
13. Bohn S, Pauchard L, Couder Y (2005) Hierarchical crack pattern as formed by successive domain divisions. I. Temporal and geometrical hierarchy. *Phys Rev E* 71:046214.
14. Bohn S, Platkiewicz J, Andreotti B, Adda-Bedia M, Couder Y (2005) Hierarchical crack pattern as formed by successive domain divisions. II. From disordered to deterministic behavior. *Phys Rev E* 71:046215.
15. Hutchinson J W, Suo Z (1992) Mixed-mode cracking in layered materials. *Adv Appl Mech* 29:63–191.
16. French J W (1925) The fracture of homogeneous media. *Trans Geol Soc Glasgow* 17:50–68.
17. Müller G (1998) Starch columns: Analog model for basalt columns. *J Geophys Res* 103:15239–15253.
18. Toramaru A, Matsumoto T (2004) Columnar joint morphology and cooling rate: A starch-water mixture experiment. *J Geophys Res* 109:B02205.
19. Goehring L, Morris S W (2005) Order and Disorder in Columnar Joints. *Europhys Lett* 69:739–745.
20. Mizuguchi T, Nishimoto A, Kitsunezaki S, Yamazaki Y, Aoki I (2005) Directional crack propagation of granular water systems. *Phys Rev E* 71:056122.
21. Goehring L, Lin Z, Morris S W (2006) An Experimental Investigation of the Scaling of Columnar Joints. *Phys Rev E* 74:036115.
22. Long P E, Wood B J (1986) Structures, textures and cooling histories of Columbia River basalt flows. *Geol Soc Am Bull* 97:1144–1155.
23. DeGraff J M, Aydin A (1987) Surface morphology of columnar joints and its significance to mechanics and direction of joint growth. *Geol Soc Am* 99:605–617.
24. Budkewitsch P, Robin P-Y (1994) Modelling the evolution of columnar joints. *J Volcanol Geotherm Res* 59:219–239.
25. Goehring L , Morris S W (Accepted July 2008) The scaling of columnar joints in basalt. *J Geophys Res* 16 pp.
26. Hardee H C (1980) Solidification in Kilauea Iki lava lake. *J Volcanol Geotherm Res* 7:211–223.
27. Hooper P R, Kawkesworth C J (1993) Isotopic and geochemical constraints on the origin and evolution of the Columbia River Basalt. *J Petrology* 34:1203–1246.

28. Reidel S P, Tolan T L, Hooper P R, Beeson M H, Fecht K R, Bentley R D, Anderson J L (1989) The Grande Ronde Basalt, Columbia River Basalt Group; Stratigraphic descriptions and correlations in Washington, Oregon, and Idaho. *Geol Soc Am Spec Paper* 239:21–53.

29. Green N L (1981) Geology and petrology of Quaternary volcanic rocks, Garibaldi Lake area, Southwestern British Columbia: summary. *Geol Soc Am Bull* 92:697–702.

30. Bye,A, Edwards B R, Hickson C J (2000) Preliminary field, petrographic, and geochemical analysis of possible subglacial, dacite volcanism at the Watts Point volcanic centre, southwestern British Columbia. *Geol Soc Canada, Curr Res* A20:1–9.

31. Russell J K, Hickson C J, Andrews G (2007) in *Floods, Faults, and Fire: Geological field trips in Washington State and Southwest British Columbia: Geological Society of Americal Field Guide 9*, eds. Stelling P, Tucker D S (The Geological Society of America), pp. 1–29.

32. Kerr A C (1998) On the nature of the parental magma of the Palaeogene Staffa Magma sub-type, Isle of Mull, Scotland. *Trans R Soc Edinburgh* 89:87–93.

33. Ryan M P, Sammis C G (1978) Cyclic fracture mechanisms in cooling basalt. *Geol Soc Am Bull* 89:1295–1308.

34. Grossenbacher K A, McDuffie S M (1995) Conductive cooling of lava: columnar joint diameter and stria width as functions of cooling rate and thermal gradient. *J Volcanol Geotherm Res* 69:95–103.

35. Rice J R, Cleary M P (1973) Some basic stress diffusion solutions for fluid-saturated elastic porous-media with compressible constituents. *Rev Geophys* 14:227–241.

36. Jagla E A, Rojo A G (2002) Sequential fragmentation: The origin of columnar quasihexagonal patterns. *Phys Rev E* 65:026203.

37. Pel L, Landman K, Kaasschieter E F (2002) Analytic solution for the non-linear drying problem. *Int J Heat Mass Transfer* 45:3173–3180.

38. Jenkins D R (2005) Optimal spacing and penetration of cracks in a shrinking slab. *Phys Rev E* 71:056117.

39. Sletten R S, Hallet B, Fletcher R C (2003) Resurfacing time of terrestrial surfaces by the formation and maturation of polygonal patterned ground. *J Geophys Res* 108:8044.

40. Shoreland-Ball S, Sparks R, Murphy M, MacNiocaill C, Daniel B Columnar jointed tuffs below a doleritic sill, Tideswell Dale, Derbyshire. *Unpublished work*